Protein Dynamics: From the Native to the Unfolded State and Back Again

MARTIN KARPLUS, AMEDEO CAFLISCH, ANDREJ ŠALI, and EUGENE SHAKHNOVICH
Department of Chemistry, 12 Oxford Street, Harvard University, Cambridge, Massachusetts 02138, U.S.A.

Abstract. Simulations to study protein unfolding and folding were performed. The unfolding simulations make use of molecular dynamics and treat an atomic model of barnase in aqueous solvent. The cooperative nature of the unfolding transition and the important role of water are described. The folding simulations are based on a bead model of the protein on a cubic lattice. It is shown for the 27-mer model that a large energy gap between the lowest energy (native) state and the excited states is a necessary and sufficient condition for fast folding.

Key words. Molecular dynamics, barnase denaturation.

I. Introduction

The dynamics of proteins includes a wide range of length and time scales [1]. Figure 1 shows a schematic diagram of the energy of a protein as a function of a configurational coordinate, such as the radius of gyration. There is the native state, which includes fluctuations of up to 2 Å in length on a time scale in the picosecond to nanosecond range. Many molecular dynamics simulations have explored this region of conformational space [2], which is of importance for protein function. A second region involves the transition from the native state to a compact globule, which may be an intermediate of the 'molten globule' type that is of great current interest [3]. Here the length scale is in the range 2–5 Å and the time scale of the motions involved is in the nanosecond to microsecond range. Finally, there are the vast number of configurations of the denatured (coil) state and the folding process from the coil to the compact globule with near native conformation. In this region the length scales are on the order of 10–20 Å and the time scales are in the microsecond to millisecond range. This paper briefly reviews some recent studies that explore the native to globule transition in barnase [4, 5] and makes use of a lattice model to study the folding process from the denatured to the organized globule state [6, 7].

II. Barnase Denaturation

Molecular dynamics simulations of the initial stages of unfolding of barnase (a 110 amino acid ribonuclease from *Bacillus amyloliquefaciens*) have been made at high temperature in the presence of water [4, 5]. This protein is a particularly good system for such studies because transition states and pathways of barnase folding and unfolding have been investigated by protein engineering and NMR hydrogen-

A. Pullman et al. (eds.), Modelling of Biomolecular Structures and Mechanisms, 69–84.

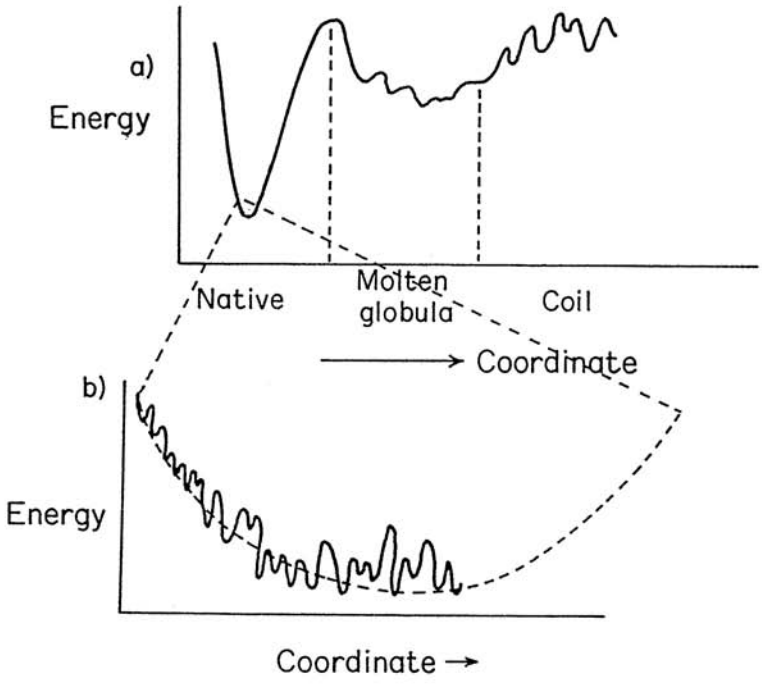

Fig. 1. Schematic representation of the configuration space of a protein giving the energy as a function of a configurational coordinate: (a) complete space; (b) enlarged view in the vicinity of the native state.

exchange trapping experiments [8]. The rate determining step for both folding and unfolding involves the crossing of a free energy barrier near the native state [9,10]. Figure 2 shows a schematic drawing of the barnase structural elements. The present simulations provide a detailed mechanism for solvent denaturation of the secondary structure and the hydrophobic cores.

The barnase denaturation simulations used a deformable boundary potential [10,11] and standard molecular dynamics methodology [2]. The system consisted of 1091 protein atoms and 3003 water molecules in a sphere of 30 Å radius. Two denaturation simulations were performed at 600 K (A600, 120 ps; R600, 230 ps) and a 300 K control trajectory was run for 250 ps. R600 was recently continued to 250 ps; in addition, a third simulation at 600 K (200 ps) was performed and analyzed (Caflisch & Karplus, in press). The denaturation process is similar in the three 600 K simulations. The 600 K temperature was used to speed up the unfolding transition. An increase in the unfolding rate by many orders of magnitude should result since the activation energy is expected to be large; the activation free energy for unfolding is 20 kcal/mol [12].

The radius of gyration (R_g) and heavy-atom root-mean-square deviation (RMSD) from the X-ray structure as a function of time are given in Figure 3. In A600 and R600, R_g starts to increase after 30 ps, while the RMSD increases immediately. Both R_g and RMSD then increase over most of the simulation.

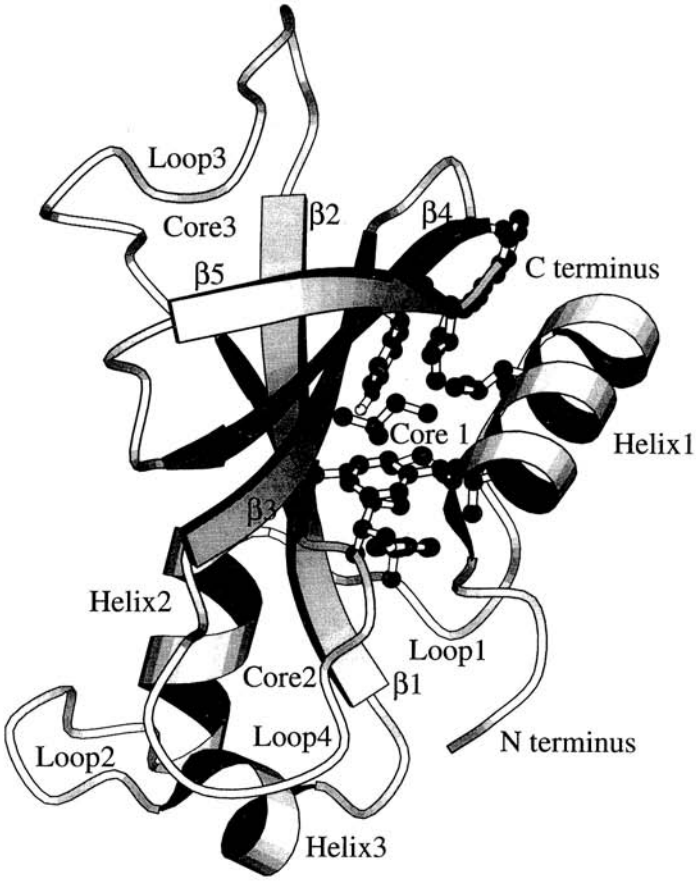

Fig. 2. Schematic picture of the backbone of barnase, emphasizing the secondary structural elements; sidechains of hydrophobic $core_1$ are plotted in a ball–and–stick representation. The structural elements include the following residues: N-terminus (1–5), $helix_1$ (6–18), $loop_1$ (19–25), $helix_2$ (26–34), $loop_2$ (35–40), $helix_3$ (41–45), type II β-turn (46–49), $strand_1$ (50–55), $loop_3$ (56–69), $strand_2$ (70–75), $loop_4$ (76–84), $strand_3$ (85–90), type I β-turn (91–94), $strand_4$ (95–100), type III′ β-turn (101–104), $strand_5$ (105–108), C-terminus (109–110). Drawn with the program.

However, the increase is not uniform; e.g. in A600, R_g is nearly constant for 20 ps between 45 and 65 ps; this may be indicative of an intermediate [13]. In the control simulation at 300 K, R_g shows a very small increase (the average R_g is 13.7 Å, relative to the X-ray value of 13.6 Å); the RMSD from the X-ray structure is 1.9 Å (the mainchain atom RMSD is 1.5 Å) during the last 50 ps.

In the A600 simulation (120 ps) and the first half (115 ps) of the R600 simulation, there are similar structural changes. The N-terminus, $loop_1$ and $loop_2$ begin to unfold during the first 30 ps. This is followed by partial denaturation of the hydrophobic cores; $core_2$ denatures relatively rapidly, followed by $core_1$, $core_3$ and $loop_3$ in both 600 K simulations. The solvation of hydrophobic $core_1$ is coupled with a large distortion of $helix_1$ and of the edge strands of the β-sheet. Both $helix_1$

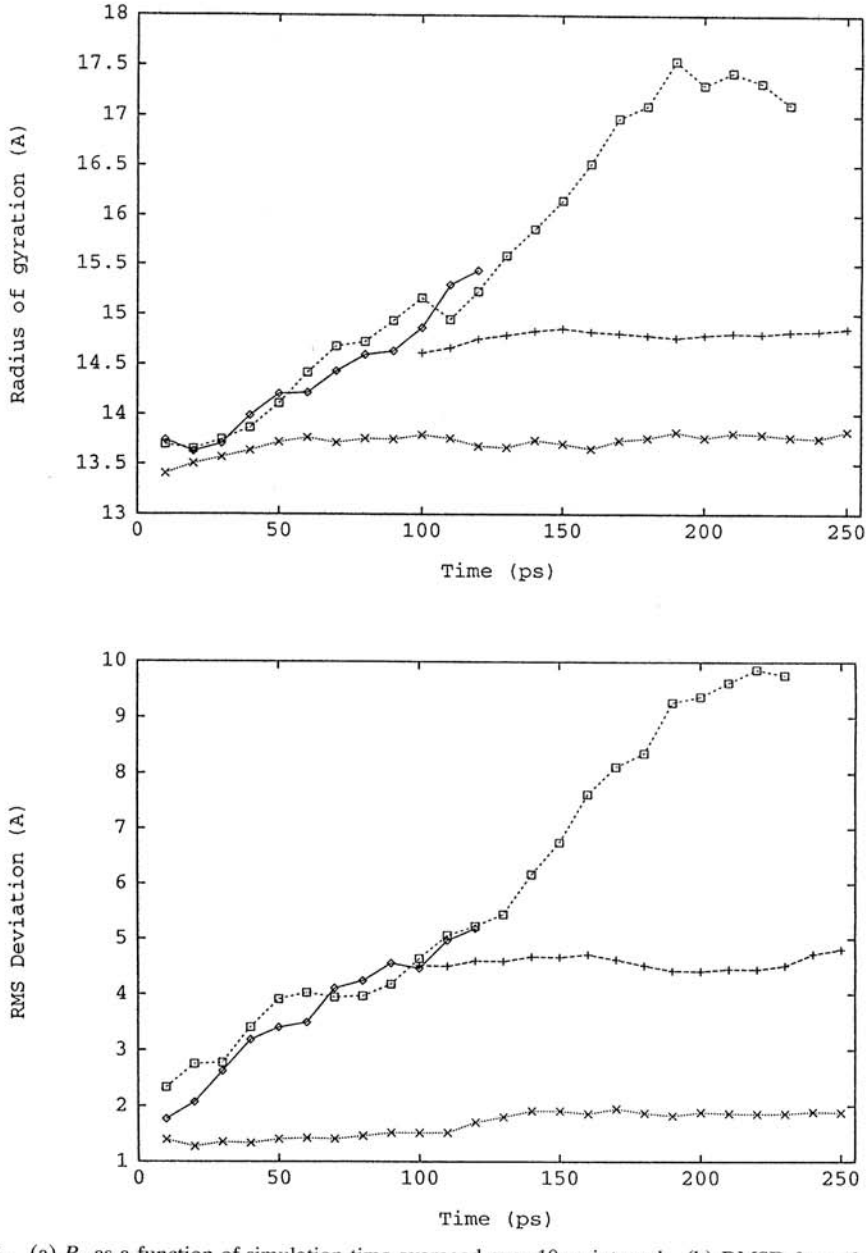

Fig. 3. (a) R_g as a function of simulation time averaged over 10-ps intervals. (b) RMSD from the X-ray structure as a function of simulation time averaged over 10-ps intervals: (——) A600, (--+-+) B300, (--□--) R600, (··×··) control run at 300 K.

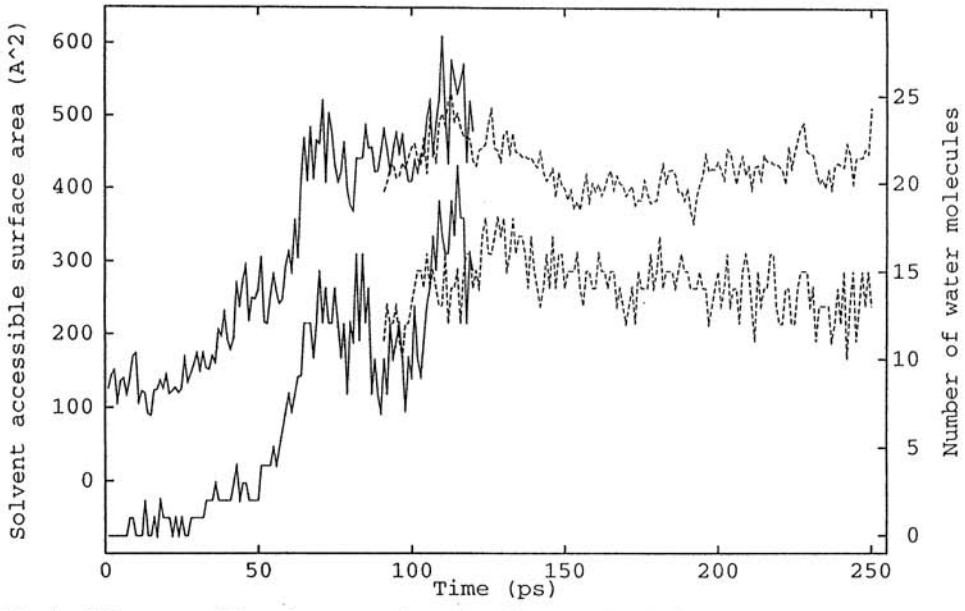

Fig. 4. Solvent accessible surface area and number of water molecules for $core_1$ as a function of time. (——) A600; (------) B300. For the exposed surface area, shown in the upper curve with the scale in $Å^2$ on the left, the Lee and Richards algorithm (CHARMM implementation) and a probe sphere of 1.4 Å radius were utilized. For the number of water molecules, shown in the lower curve with the scale on the right, those within 7 Å of the center of the core (the instantaneous center of geometry of the carbon atoms of the sidechains of residues Phe 7, Val 10, Ala 11, Leu 14, Leu 20, Tyr 24, Ala 74, Ile 76, Ile 88, Tyr 90, Trp 94, Ile 96, Ile 109) were included.

and $helix_2$ lose about half of the native α-helical hydrogen bonds; $helix_3$ unfolds after about 20 ps. In the β-sheet, about half of the native interstrand hydrogen bonds have disappeared after 100 ps; in R600 the β-sheet is fully solvated after 150 ps. During the last 50 ps of R600, the mainchain still shows essentially the same overall fold as in the native structure, although the polypeptide chain is almost fully solvated and all of the secondary structure is lost except for the last two turns of $helix_1$.

$Core_1$, which is an important stabilizing element of barnase [8,10], is formed by the packing of $helix_1$ against the β-sheet and is centered around the sidechain of Ile 88 (Figure 2). Figure 4 shows the time dependence in A600 of the solvent accessible surface area of the sidechains of $core_1$ and the number of water molecules in the core; similar behavior is seen during the first half of the R600 trajectory. Increase in accessible surface area and water penetration are nearly simultaneous and begin at about 35 ps. Sixteen water molecules have penetrated at 82 ps; this falls to 10 between 89–98 ps and increases to 17 in the period from 111 to 120 ps. Many of the solvating waters make hydrogen bonds to waters outside the core. The accessibility of $core_1$ to water is coupled with the relative motion of $helix_1$ and the β-sheet (see Figure 5); i.e., they begin to move apart at about 30 ps and their separation is continuous during the 30–80 ps period; between 80

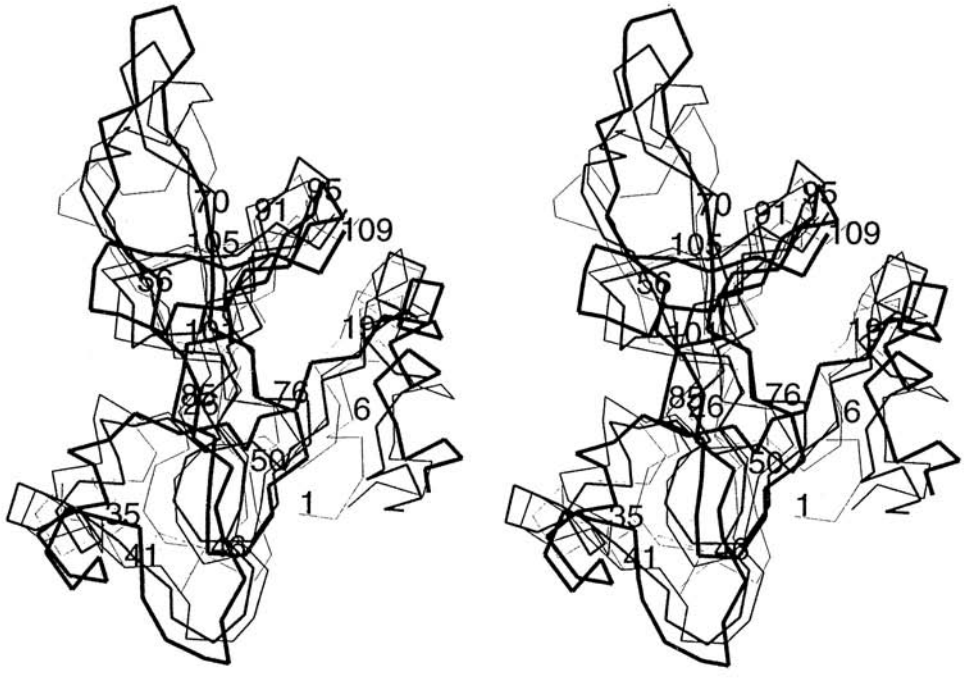

Fig. 5. Stereo view of the barnase C_α atoms to illustrate the relative $helix_1/\beta$-sheet motion during A600. 1 ps (thin line and labels), 70 ps (medium line), 90 ps (thicker line), 120 ps (thick lines).

and 100 ps there is a small closing movement in accord with the decrease of water in the core, followed by expansion for the remainder of the simulation. During the B300 simulation the number of water molecules in $core_1$ and the solvent accessible surface area of its sidechains are nearly constant (see Figure 4); the average number of water molecules is 14. This steady state of solvation of the core is correlated with the nearly constant number of hydrogen bonds in $helix_1$ and the central part of the β-sheet (strands 2–3 and 3–4).

A number of detailed results of the present analysis are of interest because they may play a role in protein denaturation, in general. The polar OH and NH groups of tyrosines and tryptophan sidechains, respectively, play an important role in the penetration of water (from the top part of $core_1$), while the motion of a lysine sidechain helps the water molecules reaching the center of $core_1$ from the bottom part (Figure 6a,b). Clusters of hydrogen bonded water molecules surrounding hydrophobic sidechains participate in hydrogen bonds with polar groups of the backbone and/or of the sidechains (Figure 6c,d). The β-sheet disruption starts near the irregular element (β-bulge at residues 53–54) and at the edges (strands 1 and 5); it is promoted by an increase in the twist and an influx of water molecules, some of which insert between adjacent strands and participate in hydrogen bonds as both donors and acceptors with the mainchain polar groups (Figure 7). Water molecules act mainly as hydrogen bonding donors in the initial phase of solvation

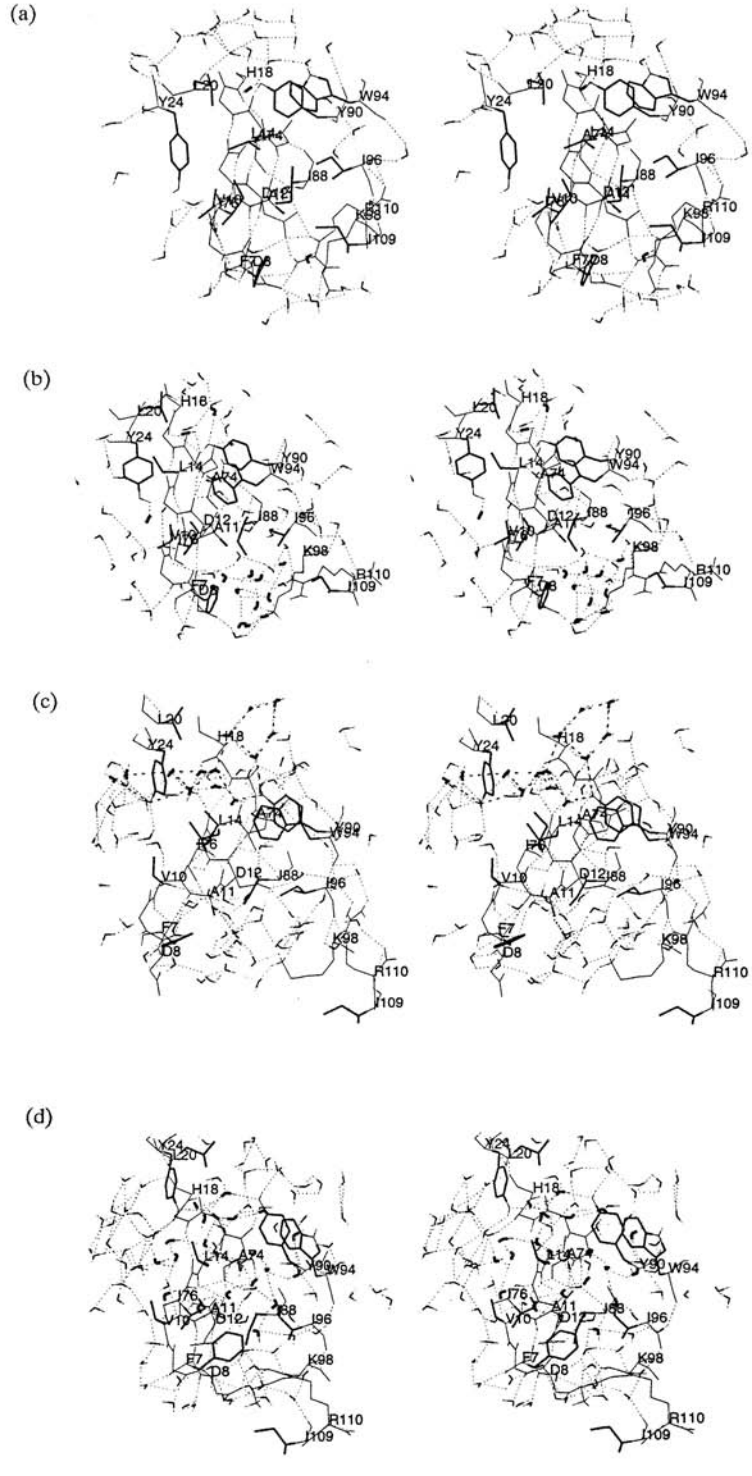
(a)
H18
L20
Y24
W94
Y90
L14
A74
I96
I88
D12
A11
V10
K98
R110
I109
F7
D8
(b)
(c)
(d)

of the main helix; sometimes they insert and replace the helical hydrogen bond, as previously found in the fragment studies [14,15].

The present results suggest a possible mechanism for the solvation of hydrophobic cores and for the dissolution of secondary structural elements in protein denaturation. Very similar results have been obtained in a simulation of acid denaturation at 365 K (Caflisch & Karplus, in press). Testing of this mechanism is a challenge for experimentalists. Techniques that make use of photo-CIDNP [16], NOEs of water interactions with specific residues [17] and chemical markers [18] are possible approaches.

III. Lattice Model for Folding and Its Implications

The essential question is how a polypeptide chain is able to fold rapidly, in ms to s, to the native state despite the very large number of conformations that exist for the denatured chain (Levinthal paradox) [19]. To approach this problem, we use a simplified model that consists of a 27-bead self-avoiding chain on a cubic lattice (Figure 8). The native (lowest-energy) state can be determined exactly [20] and a survey of the folding behavior of many sequences is possible [6,7]. In addition, the full phase space density of the system can be obtained and the thermodynamic properties can be calculated as a function of the folding reaction coordinate, which is defined as the fraction of native contacts (out of a total of 28). The model is sufficiently complex that the resolution of the Levinthal paradox is required for folding; i.e., some sequences find the native state in only $\sim 10^7$ Monte Carlo (MC) steps even though there are $\sim 10^{16}$ conformations. Since the lattice simulation does not include the amino acid sidechains, the process considered here may correspond to the folding of real proteins to the molten globule stage; i.e., the molten globule, if it has a defined fold [3], is the native state in the present model.

In the first part of the analysis, 200 sequences with random interactions were generated and subjected to MC folding simulations [6]. Of these, 30 chains found the known native state in a short time. These chains correspond to actual protein sequences in the present model; the remaining sequences, which do not fold, do not correspond to protein sequences and serve as controls. The 30 folding sequences were analyzed and compared with the non-folding sequences. Several suggested mechanisms for resolving the Levinthal paradox do not apply to the present model; i.e., the features assumed to be responsible for rapid folding are found to be the same for the folding and non-folding sequences. These include a high number of short versus long range contacts in the native state [21], a high content of secondary structure in the native state [22], a strong correlation between the native contact map and the interaction parameters [23], and the existence of

Fig. 6. Stereo views of A600 dynamics: (a) 9 ps (b) 39 ps, (c) 69 ps, (d) 115 ps. Hydrophobic sidechains of $core_1$ are shown as thick lines; α-helix backbone (residues 7–18), Asp 8, Asp 12, Lys 98, and Arg 110 sidechains are shown as thin lines. Water molecules within 12 Å of the center of geometry of $core_1$ are included. Hydrogen bonds are dotted (acceptor-hydrogen distance smaller than 2.5 Å; no angular criterion). Waters discussed in text are shown with thick lines.

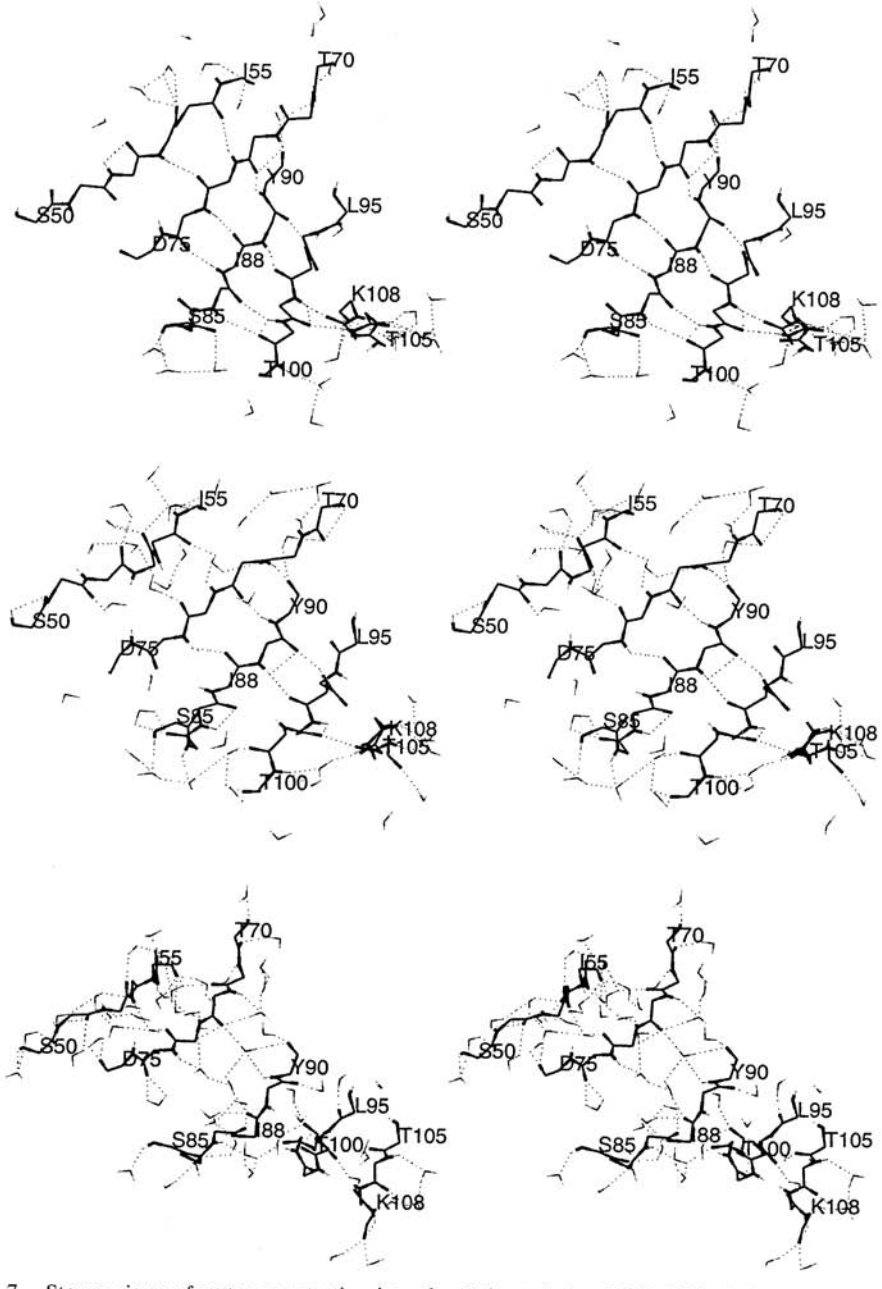

Fig. 7. Stereo views of water penetration into the β-sheet during R600. Mainchain N and O atoms are thick, hydrogens are thin and hydrogen bonds are dotted; water molecules within 3 Å of any mainchain atom of the β-sheet are shown. Top, 1 ps; middle, 60 ps; bottom 150 ps.

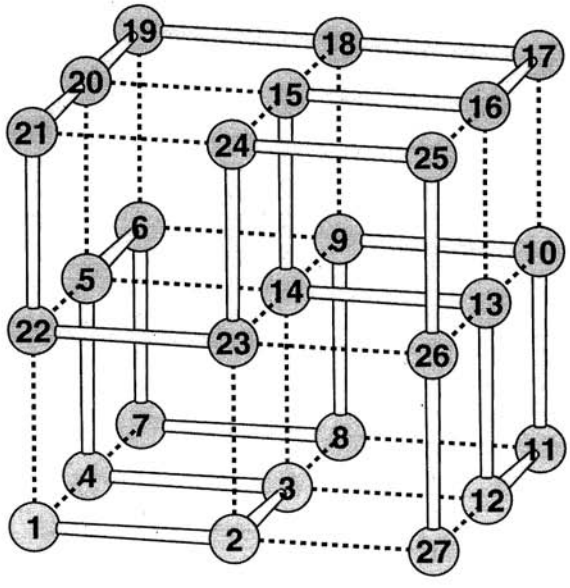

Fig. 8. Lattice model of protein folding. An example of a compact self-avoiding structure of a chain of 27 monomers (filled numbered circles) with 28 contacts (dashed lines). The total energy of a conformation is the sum of contact energies: $E = \Sigma_{i<j} \Delta(r_i, r_j) B_{ij}$, where r_i are the positions of monomers i, B_{ij} are the contact energies for pairs of monomers i, j, and $\Delta(r_i, r_j)$ is 1 if monomers i and j are in contact and is 0 otherwise; two monomers are in contact if they are not successive in sequence and at unit distance from each other. The values of the B_{ij} are obtained from a Gaussian distribution with a mean B_0 and standard deviation σ_B. The parameter B_0 is an overall attractive term that emulates the hydrophobic effect observed in globular proteins. The *native* conformation is the compact self-avoiding chain with the lowest energy.

a high number of low energy states with near-native conformations [20]. Moreover, there is no repetitive trapping of the non-folding sequences in the same local minimum, so that the native state cannot be a metastable state [24]. The only significant difference between folding and nonfolding sequences is that the native state is at a pronounced energy minimum in the former. As can be seen in Figure 9, there is a large energy gap between the native and the 'excited' states in the sequences that fold; no such gap is present in the nonfolding sequences. This energy gap is the necessary and sufficient condition for a sequence to fold rapidly in the present model.

The time history of the folding process (Figure 10) shows that there is a rapid collapse in $\sim 10^4$ MC steps to a semi-compact random globule; i.e., the number of contacts increases, the energy decreases, while the fraction of native contacts remains below 0.3. In this way, the total of $\sim 10^{16}$ random-coil conformations is reduced to $\sim 10^{10}$ random semi-compact globule states. The fast collapse results from a large energy gradient and the presence of many empty lattice points. In the second, rate limiting, stage the chain searches for one of the $\sim 10^3$ transition states. The transition region consists of all states from which the chain folds rapidly

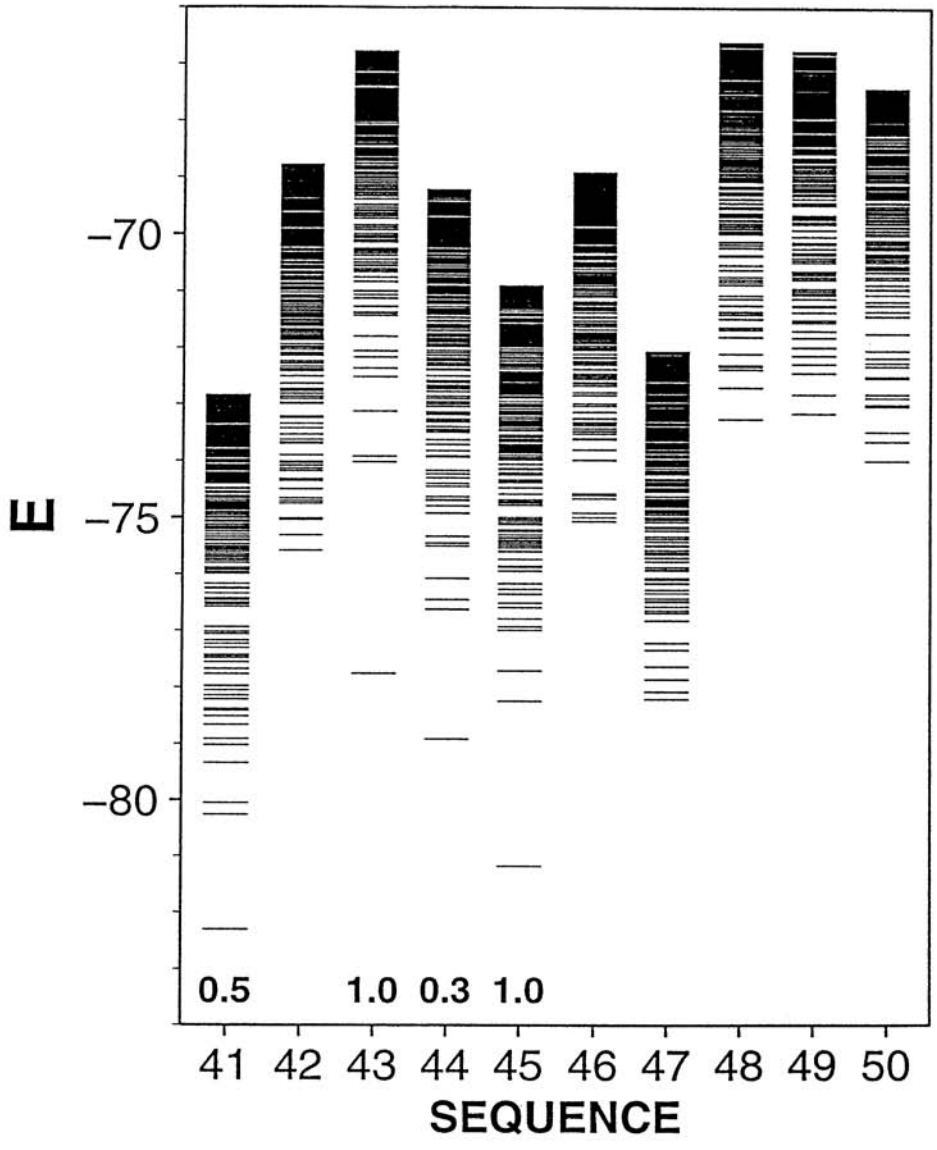

Fig. 9. Energy spectra for 10 folding and nonfolding random sequences. The energies of the 400 lowest compact self-avoiding conformations are shown. The native state corresponds to the bottom bar. The numbers below the spectra show the probabilities that the corresponding sequence will fold under the conditions of the simulation (6); if no number is given, the probability is 0.

to the native state. The transition states are structurally similar to the native state, with 23 to 26 of the native contacts. The mean first passage time, τ, for finding any of the n states among the total of N states by a random search which explores r states per unit of time is $N/(n \times r)$. For the present model, $\tau \sim 10^{10}/(10^3 \times 1) =$

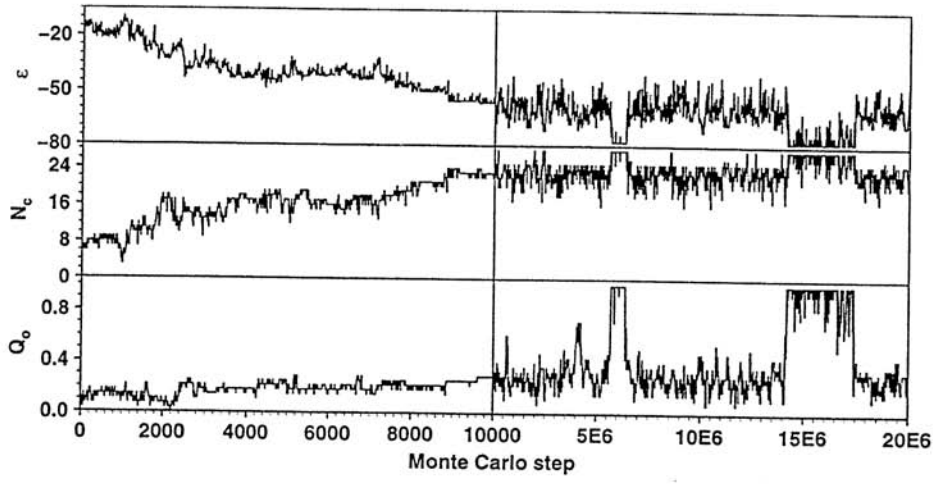

Fig. 10. Typical trajectory for a folding sequence ($T = 1.3$). Energy, ϵ (in units of $k_B T$); the number of contacts, N_c; fraction of the number of contacts in common with the native state, Q_0. The instantaneous values of these quantities are plotted every 10 MC steps in the first part of the trajectory ($\leq$10000 MC steps) and every 20000 steps in the subsequent part. The folding trajectory starts with a random-coil conformation and consists of local MC moves of one or two successive monomers that preserve bond lengths and avoid multiple occupancy of the lattice sites [6].

10^7, of the same order as the observed time scale (Figure 10). This indicates that the rate limiting stage in folding consists of a random search for a transition state in the semi-compact part of the phase space; i.e., a folding 'pathway' is not involved in finding the native state. In the third stage, the chain rapidly (within $\sim 10^5$ MC steps) attains the native conformation from any one of the transition states.

To examine the kinetics of the folding process, we write the unimolecular rate expression; i.e.,

$$\frac{dC_N}{dt} = kC_D$$

where C_N is the probability of finding the unique native state at time t, C_D is the probability of the denatured states (all other states; i.e., $C_D = 1 - C_N$) and k is the rate coefficient. Since the folding process takes place on a complex multiminimum surface, it would be possible for k not to be the usual rate constant, but a function of time [25]. To determine the kinetic behavior, we show in Figure 11 a plot of $\ln(1 - C_N) = -kt$ versus the number of MC steps, which correspond to the time in the lattice model. The probability of finding the native state at time t is estimated from 100 independent folding simulations at several temperatures. It is calculated from the distribution of first passage times (i.e., when the native state is reached for the first time). It is evident from the figure that the coefficient k is indeed a rate constant; i.e., it is independent of time. To examine the dependence of the folding rate on temperature, $\log k$ is plotted versus $1/T$ in Figure 12. This plot

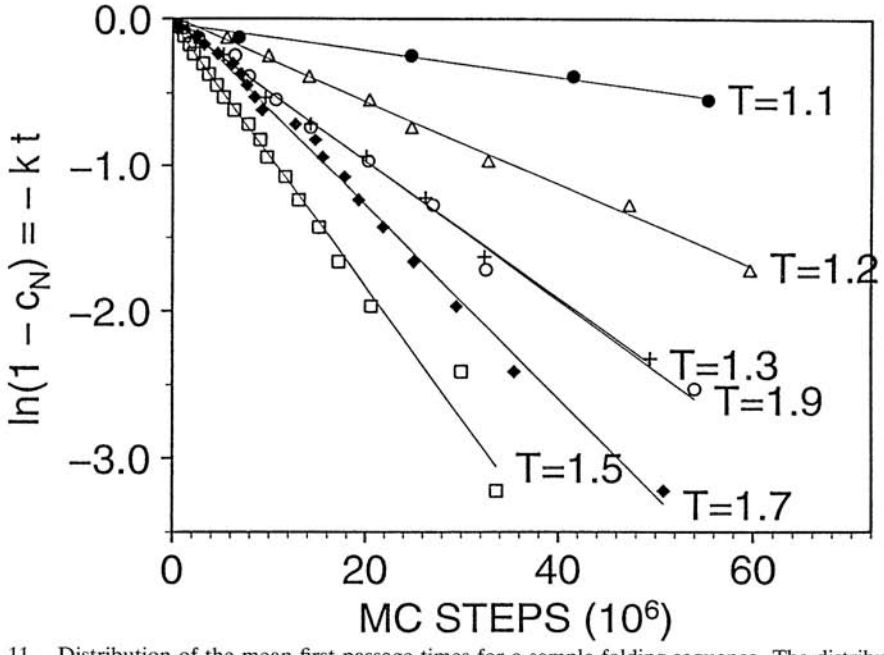

Fig. 11. Distribution of the mean first passage times for a sample folding sequence. The distribution of the mean first passage times is shown at the temperatures indicated on the plot. The lines are the linear least-squares fits to the points. 100 independent folding trials were done to obtain the points shown.

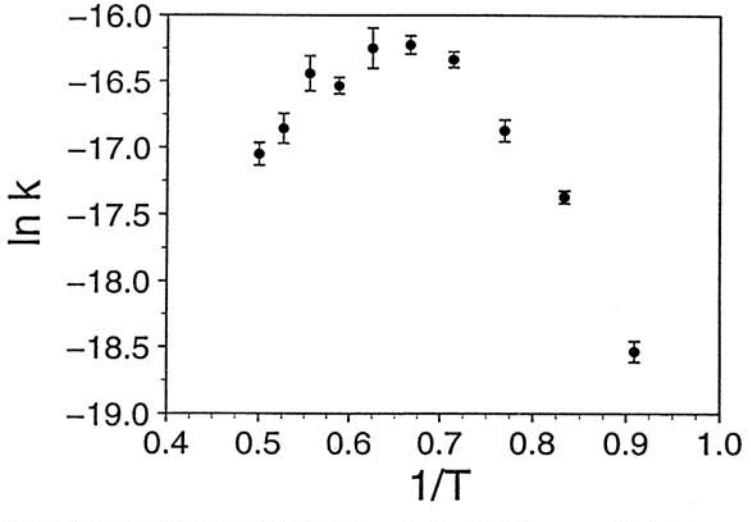

Fig. 12. Temperature dependence of the folding rate constant for a sample folding sequence. This Arrhenius plot shows the rate constants at different temperatures that were obtained from Figure 12. The standard error of this estimate was found by the jacknife test.

shows a strong deviation from standard Arrhenius type behavior. For low T ($0.90 < 1/T < 0.65$) there is an increase in the folding rate, as expected from an activation energy limited process. However, at higher T ($0.65 < 1/T < 0.50$) the rate decreases with increasing temperature as expected from an activation entropy dominated process. This is in accord with analysis of the configuration space of the system; i.e., at low temperatures, an increase in temperature makes it easier to get over the energy barriers which are rate limiting. However, at higher temperatures, a larger portion of the configuration space becomes accessible, which results in a slowing down of the folding process.

The pronounced energy minimum is the necessary condition for the folding of a 27-mer on a lattice because it guarantees that the native state is stable above the critical temperature, where the rearrangements of the structure with local unfolding required in the rate limiting stage are energetically possible. It is also a sufficient condition because a random search of compact globules with random structures can rapidly find a transition state that folds to the stable native state in a short time. While a non-folding sequence may also fold slowly to its native state above the critical temperature, it would not be stable and, therefore, could not correspond to a real protein.

The size of the search space for the native state is greatly reduced when the chain is semi-compact as it is in real proteins [26]. Nevertheless, in the 27-mer model as in real proteins, a random search of a collapsed globule cannot find the native state in the observed time. It is the existence of a transition region, consisting of a large number of states, that reduces the search time to realistic values when combined with the search of the random compact globule. Extrapolation of the folding time to real proteins suggests that the three-stage random search mechanism could be effective for small proteins (Figure 13). However, the mechanism breaks down for long chains because the folding time increases exponentially with chain length; i.e., the number of semi-compact states increases faster than the number of the transition states. Thus, a modification of the present mechanism is required for larger proteins.

It is likely that proteins existing early in evolution were small enough to fold according to the three-stage random search mechanism [27]. Since the pre-biotic and early biotic environment was hot, unusually thermostable proteins were required, such as those found in the most primitive bacteria that live at temperatures as high as 105° [28]. If so, the stability condition required a native state that corresponded to a low energy minimum for which the folding problem was solved simultaneously. As the evolution progressed, longer proteins evolved. These proteins had to fold on the same time scale. One way of achieving this is by evolving proteins with sequences that have a larger difference between the native and non-native contact energies than the random folding sequences of the present model. Such sequences would have an even more pronounced global minimum in their potential surfaces, in line with the 'consistency principle' [29] and the 'principle of minimal frustration' [30]. A factor may be the existence of a nucleus for folding [21], or the early appearance of secondary structural elements [31], neither of which are found in the present model. As a result, the collapse would not result in random semi-compact globules and the very favorable native contacts would

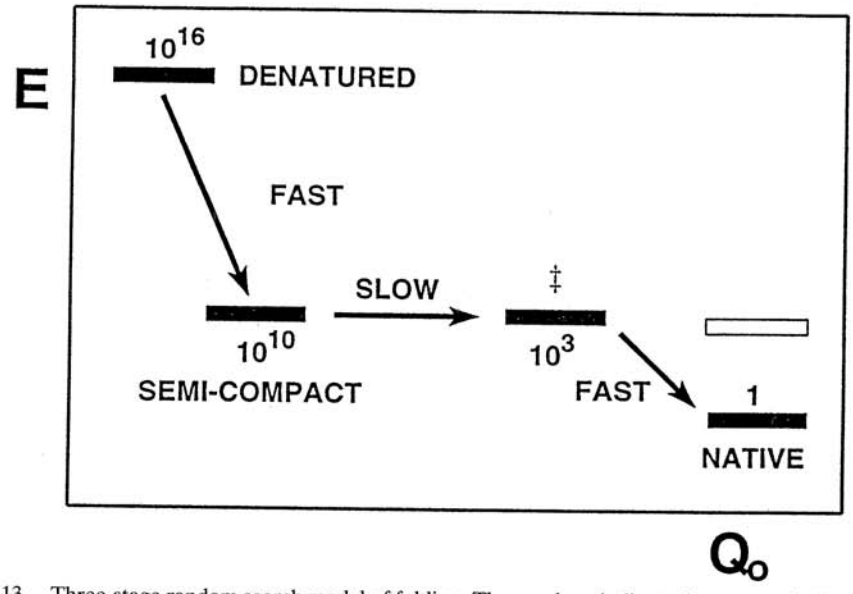

Fig. 13. Three-stage random search model of folding. The numbers indicate the geometrically possible conformations obtained from the density of states that was determined as a function of energy and reaction coordinate. The solid rectangles correspond to folding sequences. The empty rectangle indicates the energy of the native state of a nonfolding random sequence. The other states of a nonfolding sequence appear at the same positions as the corresponding states of a folding random sequence.

lead more directly to a native-like molten globule state. Actual proteins could use an intermediate mechanism that might vary with the external conditions.

The results of this study may have implications for the prediction of the structure of a protein from its amino acid sequence. The success of the three-stage random search in finding the pronounced global minimum on a potential surface suggests, at least for small proteins, that the bottleneck in structure prediction may be the derivation of a suitable potential function rather than the design of folding algorithms.

Acknowledgements

Most of the material in this paper is based on a lecture at the 27th Jerusalem Symposium (May 1994) and it was taken mainly from references 4, 6 and 7. A. Caflisch was supported by a grant from the Schweizerischer Nationalfonds. A. Sali is a Fellow of the Jane Coffin Childs Memorial Fund for Medical Research. Support was also provided by a David and Lucille Packard Fellowship (E.S.), and by a grant from the National Science Foundation and a gift from Molecular Simulations Inc. (M.K.).

References

1. M. Karplus and E. Shakhnovich: in *Protein Folding*, T. Creighton (Ed.), W.H. Freeman & Sons, p. 127 (1992).
2. C. L. Brooks III, M. Karplus, and B. M. Pettitt: *Proteins: A Theoretical Perspective of Dynamics, Structure, & Thermodynamics*, Adv. Chem. Phys. Vol. LXXI, John Wiley & Sons (1988).
3. O. B. Ptitsyn: in *Protein Folding*, T. E. Creighton (Ed.), W.H. Freeman, New York, p. 243 (1992).
4. A. Caflisch and M. Karplus: in *The Protein Folding Problem and Tertiary Structure Prediction*, K. Merz, Jr. and S. Le Grand (Eds.), Birkhäuser, Boston, MA, p. 193 (1994).
5. A. Caflisch and M. Karplus: *Proc. Natl. Acad. Sci. USA* **91**, 1746 (1994).
6. A. Šali, E. Shakhnovich, and M. Karplus: *J. Mol. Biol.* **235**, 1614 (1994).
7. A. Šali, E. Shakhnovich, and M. Karplus: *Nature* **369**, 248 (1994).
8. A. R. Fersht: *FEBS Letters* **325**, 5 (1993).
9. L. Serrano, A. Matouschek, and A.R. Fersht: *J. Mol. Biol.* **224**, 805 (1992).
10. L. Serrano, A. Matouschek, and A.R. Fersht: *J. Mol. Biol.* **224**, 847 (1992).
11. C.L. Brooks III and M. Karplus: *J. Chem. Phys.* **79**, 6312 (1983).
12. A. Matouschek, J. T. Kellis, Jr., L. Serrano, M. Bycroft and A. R. Fersht: *Nature* **346**, 440 (1990).
13. A. E. Mark and W. F. van Gunsteren: *Biochemistry* **31**, 7745 (1992).
14. J. Tirado-Rives and W. L. Jorgensen: *Biochemistry* **30**, 3864 (1991).
15. D. J. Tobias and C. L. Brooks III: *Biochemistry* **30**, 6059 (1991).
16. R. Kaptein, K. Dijkstra, and K. Nicolay: *Nature* **274**, 293 (1978).
17. G. Otting and K. Wüthrich: *J. Am. Chem. Soc.* **111**, 1871 (1989).
18. C. Ghelis: *Biophysical J.* **32**, 503 (1980).
19. C. Levinthal: in *Mossbauer Spectroscopy in Biological Systems, Proceedings of a Meeting held at Allerton House, Monticello, Illinois*, P. Debrunner, J. C. M. Tsibris, and E. Münck (Eds.), University of Illinois Press, Urbana, p. 22 (1969).
20. E. Shakhnovich, G. Farztdinov, A. M. Gutin and M. Karplus: *Phys. Rev. Lett.* **67**, 1665 (1991).
21. D. B. Wetlaufer: *Proc. Natl. Acad. Sci. USA* **70**, 697 (1973).
22. P. Kim and R. Baldwin: *Ann. Rev. Biochem.* **59**, 631 (1990).
23. N. Go and H. Abe: *Biopolymers* **20**, 1013 (1981).
24. J. D. Honeycutt and D. Thirumalai: *Biopolymers* **32**, 695 (1992).
25. Y. S. Bai and M. D. Fayer: *Phys. Rev.* **B39**, 11066 (1989).
26. K. A. Dill: *Biochemistry* **24**, 1501 (1985).
27. E. E. Di Iorio, W. Yu, C. Calonder, K. H. Winterhalter, G. De Sanctis, G. Falcioni, F. Ascoli, B. Giardina, and M. Brunori: *Proc. Natl. Acad. Sci. USA* **90**, 2025 (1993).
28. K. O. Stetter: in *Frontiers of Life*, J. K. Trân Thanh Vân, J. C. Mounolou, J. Schneider, and C. McKay (Eds.), Editions Frontières, Gif-sur-Yvette, France, p. 195 (1992).
29. N. Go and H. Abe: *Adv. Biophys.* **18**, 149 (1984).
30. J. D. Bryngelson and P. G. Wolynes: *Proc. Natl. Acad. Sci. USA* **84**, 7524 (1987).
31. H. Taketomi and N. Go: *Intl. J. Peptide Prot. Res.* **7**, 445 (1975).
32. M. Karplus and D. L. Weaver: *Protein Sci.* **3**, 650 (1994).